Journal of Chromatography A, 1225 (2012) 141–149

Contents lists available at SciVerse ScienceDirect

Journal of Chromatography A

journal homepage: www.elsevier.com/locate/chroma

Selection of stationary phase particle geometry using X-ray computed tomography and computational fluid dynamics simulations☆

Irma Schmidt*, Mirjana Minceva, Wolfgang Arlt

Chair of Separation Science and Technology, Friedrich-Alexander University Erlangen-Nuremberg, Egerlandstr. 3, 91058 Erlangen, Germany

ARTICLE INFO

Article history:
Received 21 September 2011
Received in revised form
14 December 2011
Accepted 21 December 2011
Available online 3 January 2012

Keywords:
Chromatography
Stationary phase
Particle geometry
X-ray computed tomography
CFD simulation

ABSTRACT

The X-ray computed tomography (CT) is used to determine local parameters related to the column packing homogeneity and hydrodynamics in columns packed with spherically and irregularly shaped particles of same size. The results showed that the variation of porosity and axial dispersion coefficient along the column axis is insignificant, compared to their radial distribution. The methodology of using the data attained by CT measurements to perform a CFD simulation of a batch separation of model binary mixtures, with different concentration and separation factors is demonstrated. The results of the CFD simulation study show that columns packed with spherically shaped particles provide higher yield in comparison to columns packed with irregularly shaped particles only below a certain value of the separation factor. The presented methodology can be used for selecting a suited packing material for a particular separation task.

1. Introduction

In recent times preparative liquid chromatography earns an important role in the field of bioproducts as well as in the field of pharmaceuticals. As it offers higher selectivity in comparison to the conventional separation methods like distillation and extraction this separation technique is already a well established part of the downstream processing. To obtain high separation resolution and to run the process economically, the columns need to have high efficiency. Three parameters are affecting the separation performance: adsorption thermodynamics, mass transfer kinetics and hydrodynamics. This work focuses on the influence of hydrodynamics on the separation efficiency.

Column efficiency and homogeneity of the column packing are directly linked. The more homogeneous the packed bed the flatter the flow profile, and thus the better the desired plug flow behavior is approached [1–5]. In columns with high packing homogeneity, the peaks will be narrow and the peak resolution better than in a column with lower packing homogeneity. It is well known that the packed bed of a chromatographic column is heterogeneous. In literature there is much evidence describing this fact [3–11]. One of the main reasons for this inhomogeneity is friction between the wall and particles during packing the column. A non-homogeneous arrangement of the particles in the vicinity of the wall and between the particles itself causes a different distribution of stress and strain inside the packing. The so-called wall effect, which occurs when rigid particles are used as a stationary phase, leads to different properties of the column packing along the radial position in the column [12–14]. This feature has been proven by the authors in former works [3–5]. The wall region normally ranges from 10 to 50 particle diameter [2,15]. Axial and radial heterogeneities not only occur because of the wall effect but also due to packing instabilities [16]. The consequences are channeling or dead volumes in the column packing, which influence the plug flow adversely [17].

In literature, several recent works are available dealing with the influence of hydrodynamic parameters on the columns efficiency [33–35]. As a chromatographic column is a closed system, the acquisition of data necessary for evaluating the column performance is just possible at the column outlet. The values obtained are averaged values along the whole column length and do not give any information about local inhomogeneities. This fails to represent the three dimensional object and no conclusions can be made on the influence of locally distributed heterogeneities on the column efficiency in total. By using conventional measuring devices, like for example velocity probes, the flow of the mobile phase would be disturbed and the values obtained would not represent the values for existing flow pattern. For process improvement and its optimization reliable experimental data are needed.

A general overview of different non-invasive measuring techniques can be found in [23]. Nuclear Magnetic Resonance (NMR)

☆ Presented at the 24th International Symposium on Preparative and Process Chromatography, Boston, MA, USA, 10–13 July 2011.

* Corresponding author. Tel.: +49 9131 8527455; fax: +49 9131 8527441.
E-mail address: irma.schmidt@cbi.uni-erlangen.de (I. Schmidt).

0021-9673/$ – see front matter © 2012 Elsevier B.V. All rights reserved.
doi:10.1016/j.chroma.2011.12.072

tomography is one of the techniques already used for studying relevant chromatographic parameters [18–21,22]. The main disadvantage of this technique is that equipment made of metal (i.e. tubes, valves, pumps) cannot be used. Our group is pioneer in using X-ray computed tomography (CT) as a novel non-invasive measuring technique for the determination of chromatographic data inside packed beds [3]. In our previous works [3–5], the influence of the packing pressure, particle shape and size as well as the ratio between the column diameter and particle diameter on the packing structure and its homogeneity was studied in details. The overall results have shown that the bed porosity and axial dispersion coefficient are distributed over the column cross sectional area and are pronounced to a larger extent in columns packed with irregularly shaped particles.

Considerable numbers of studies on the simulation of flow through porous media is available in literature [33,36–40]. There are different approaches to reconstruct the bed packing. On the one hand the bed is generated by using defined or random arrangements of single particles in a column. On the other hand, the porous structure of a packed bed is reproduced by implementing into computational fluid dynamic (CFD) software a distribution of relevant fluid mechanical parameters. The authors use in their CFD simulations the latter mentioned option. It was shown in detail in the previous works [3–5] how the data obtained from the CT experiments describing the porosity and axial dispersion coefficient distribution could be used for simulating a real separation process of a binary model mixture, taking into account adsorption thermodynamics and mass transport phenomena, respectively.

The axial distribution of the column packing plays an important role in column separation performance as shown in literature [24]. Even though, the variation of the packing density in axial direction is low and its extent small over the whole column length [25] it has to be proven whether one must account for this in the simulation model.

In this work, at first, the variation of porosity and axial dispersion coefficient in axial direction in columns packed with spherically and irregularly shaped particles was closely studied by means of CT. The attained data were implemented into a CFD model and used to simulate a batch separation of a binary mixture. Two different particle sizes were studied and their impact on the yield of the separation was estimated for different sample concentrations and separation factors. At the end, it was shown how packing and hydrodynamics parameters acquired by CT can be used to select a suited stationary phase for a given separation task.

2. Experimental

2.1. Materials

Glass columns with an inner diameter of 26 mm (Götec – Labortechnik, Germany) were used in the experiments. The packing procedure is described in more details in [5]. Two reversed silica stationary phases of different shape but similar size were used. Their commercial names and geometrical characteristics are listed in Table 1. The particle porosity was measured using a titration method described by Mottlau [26]. Both stationary phases have approximately same particle porosity and a pore diameter of 100 Å, thus similar intraparticle mass transfer kinetics would be expected.

Two mobile phases were used. One mobile phase was pure methanol; the other was a solution of potassium iodine (the tracer) in pure methanol. It was assumed that the ionic tracer does not interact with the surface of the particles. The tracer attenuates X-ray beams in a higher degree compared to the pure mobile phase and therefore the two mobile phases could be distinguished in the column by CT.

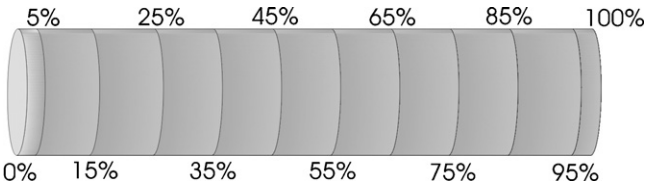

Fig. 1. Monitoring positions along the column axis.

2.2. Experimental setup and procedure

The experiments were performed with a CT-Scanner (Somatom Plus of 4th generation, Siemens). The chromatographic column was mounted at the patient table and could be moved along its axis. In order to study the axial distribution of the column packing, several monitoring positions were chosen. The part of the column between two monitoring position presents one segment in the column. Fig. 1 shows the subdivision of the column length in its single segments.

In each run four positions were scanned. So, in total, three experimental runs were carried out to scan all 12 monitoring positions along the column. The first run includes the positions of 5%, 35%, 65% and 95% of the column length. The second run covers the positions at nearly 0%, 25%, 55% and 85% of the column length. In the last experimental run the positions at 15%, 45%, 75% and approximately at 100% of the column length were scanned. Thus, the column was separated into eleven segments. For the study of the relevant parameters in axial direction the first segment, in between 0% and 5%, and the last segment, between 95% and 100% of the column length, were not taken into account. The experimental data acquired at the column inlet and outlet were influenced by the presence of the flow distributor and filter, which have caused artifacts on the CT images. Multiple experimental runs on one column, covering different positions along the column axis were justified, as the reproducibility was proven in former experiments.

At first, the column was saturated with pure methanol and scans were taken at the monitoring positions along the column as described above. In the next step, the second mobile phase (tracer dissolved in methanol) was pumped into the column and the breakthrough at defined positions was monitored. In the end, again scans were taken at the above mentioned positions of the column saturated with the second mobile phase. In Fig. 2 a series of CT images taken at a fixed monitoring position during three stages of the experimental procedure is shown. Fig. 2a represents the column cross section saturated with pure methanol. In Fig. 2c the column cross section is saturated with the tracer solution. Fig. 2b shows one image of the breakthrough of the tracer at a certain degree of saturation.

The column packing is displayed in gray color; the white ring enclosing it represents the glass column. The black ring between the column wall and column packing is an artifact which appears at the contact surface between two materials (glass and stationary phase) with a significantly different attenuation of the X-ray beams. In this region the data for image reconstruction cannot be calculated correctly.

The CT number is a normalized dimensionless parameter. Every pixel on a CT image is related to a CT number. Since the resolution of the scanner is not high enough, single particles cannot be resolved. Thus one pixel of the CT image includes the stationary phase together with the mobile phase. The CT number represents an average weighted number of the CT numbers of the mobile and the stationary phase:

$$CT_{SP/MP_1} = \varepsilon \cdot CT_{MP_1} + [(1-\varepsilon) \cdot CT_{SP}] \quad (1)$$

CT_{SP/MP_1} and CT_{SP/MP_2} are the CT numbers of the two reference scans of the column saturated with pure methanol (CT_{SP/MP_1}) and

Table 1
Stationary phases and their geometrical properties.

Name	Producer	Mean diameter d_p [μm]	Particle porosity ε_P [–]	d_{90}/d_{10}
Spherical material				
YMC-Gel ODS-A S-50 μm	YMC, Japan	46.4	0.489	2.49
Irregular material				
Lichroprep 40–63 μm	Merck, Germany	49.7	0.409	3.24

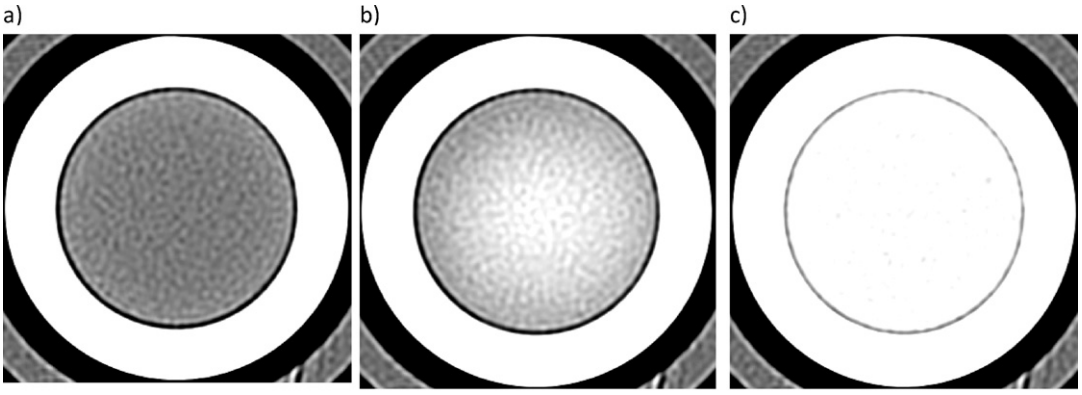

Fig. 2. CT-images of the column cross section of a column packed with spherically shaped particles showing the mobile phase transition; (a) pure methanol, (b) breakthrough of the tracer solution and (c) tracer solution.

tracer solution (CT_{SP/MP_2}), which are presented in Fig. 2a and c, respectively. In breakthrough experiments the CT number is a time dependent parameter, CT(t), defined by Eq. (2).

$$CT(t) = \varepsilon \cdot [(1 - S) \cdot CT_{MP_1} + S \cdot CT_{MP_2}] + [(1 - \varepsilon) \cdot CT_{SP}] \quad (2)$$

Combining Eqs. (1) and (2) and rearranging them, the saturation S(t) or normalized concentration c/c_0 can be calculated (Eq. (3)).

$$S(t) = \frac{c}{c_0} = \frac{CT(t) - CT_{SP/MP_1}}{CT_{SP/MP_2} - CT_{SP/MP_1}} \quad (3)$$

Using Eq. (3), the degree of saturation at a given monitoring position during the tracer breakthrough can be determined.

The locally measured breakthrough curves can be used for the calculation of different local column parameters. In [3–5] a detailed description of the procedure used for the treatment of the data obtained by CT experiments is given.

3. Results

This section is organized in two parts. In the first part the method used to derive column packing related parameters (column porosity and axial dispersion) from the data obtained from the CT experiments is presented. The axial distribution of these parameters in a column packed with particles of different geometry is shown and analyzed. In the second part, it is demonstrated how the data obtained from the CT experiment (local values of porosity and axial dispersion) can be integrated in a CFD model of a chromatographic column. In the end, it is shown how this model can be used to study the column separation performances and to select the most appropriate particle geometry for a specific separation task.

3.1. Determination of the local column porosity and axial dispersion

The columns used in the experiments were packed by applying packing pressure of 20 bar [4]. The column packed with spherically shaped particles had a bed length of 305 mm; the column bed made out of particles with an irregular shape had a bed length of 287 mm. Tracer breakthrough experiments were carried out at two different flow rates, 3 and 6 ml/min.

3.1.1. Mathematical treatment of CT images

To derive chromatographic data the images obtained by CT measurements had to be processed mathematically. According to Eq. (3), the evaluation of CT images taken at a given monitoring position over the whole column cross section would provide a global breakthrough curve excluding the radial dependency. To be able to describe the radial distribution, the column cross section was divided into 40 annuli of same area [5]. As mentioned above, to account for the axial distribution, the column length was divided into nine segments of same length. A schematic presentation is shown in Fig. 3.

For each single annulus at a given monitoring position, an individual breakthrough curve was calculated by Eq. (3). Using the method of moments [27], the retention time t_R and the variance σ^2 of each breakthrough curve were determined. These parameters were used for further calculations. As the monitoring positions were consecutively arranged, and the distance Δz between the two positions was known, the effective velocity of the tracer could be calculated in each annulus and segment.

$$v_{KI}(r) = \frac{\Delta z}{t_{R,i+1}(r) - t_{R,i}(r)} \quad (4)$$

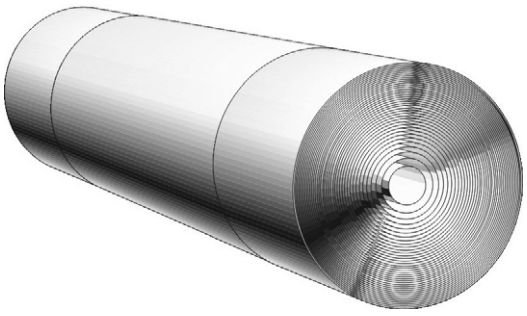

Fig. 3. Schematic presentation of a chromatographic column with column cross section divided into 40 annuli of same area and three segments.

Index i denotes the number of the monitoring position. For each segment between two monitoring positions 40 velocities (one for each annulus or overall 360 velocities for the nine segments along the column axis) were obtained using Eq. (4). The average velocity of the tracer, $\bar{v}_{KI}$, in one segment (between two monitoring positions), was calculated as follows:

$$\bar{v}_{KI} = \frac{\sum_{i=1}^{n} v_{KI}(r)}{n}, \quad n = 40 \tag{5}$$

The averaged total porosity ε_t of one segment could be calculated according to Eq. (6).

$$\varepsilon_t = \frac{\dot{V}}{A_C \cdot \bar{v}_{KI}} \tag{6}$$

The external porosity of one segment was determined using Eq. (7), wherein ε_t is the calculated total porosity by Eq. (6) and ε_p the particle porosity, given in Table 1.

$$\varepsilon = \frac{\varepsilon_t - \varepsilon_P}{1 - \varepsilon_P} \tag{7}$$

As described in Ref. [27], in order to save experimental time and effort, the radial distribution of the local external porosity was calculated using the equation of Blake–Kozeny (Eq. (8)).

$$\frac{\Delta p}{L} = \frac{150 \cdot \mu \cdot (1 - \varepsilon(r))^2 \cdot u_0(r)}{(\varepsilon(r))^3 \cdot d_p^2} \tag{8}$$

Here u_0 is the superficial velocity, calculated from the tracer velocity v_{KI} in each annulus and segment and the total porosity $\varepsilon_t(u_0(r) = v_{KI}(r) \cdot \varepsilon_t)$. Since there were two unknown parameters, the pressure drop, Δp, and the external porosity, ε, an iteration step was used to solve this equation. First, a value for the pressure drop was preset and the external porosity for each single annulus and segment was determined. After averaging the 40 single values of external porosity in one segment, the average external porosity was calculated. This value was then compared to the value of porosity calculated from Eq. (7). If the two values were in agreement the iteration stopped, otherwise a new value for the pressure drop was preset and the iteration started again. At the end of the iteration the radial distribution of the external porosity in one segment was obtained. This method was valid, as the flow regime in the column was in the laminar range [28], more details are available in [29].

Another important parameter to describe the column efficiency is the height equivalent to a theoretical plate (HETP). This parameter could be used to calculate the axial dispersion in each annulus in one segment of the column, according to following general equation:

$$\mathrm{HETP}(r) = \frac{L}{N(r)} = \frac{L \cdot \sigma^2(r)}{t_R^2(r)} = \frac{2 \cdot D_{ax}(r)}{u(r)} \tag{9}$$

Eq. (9) can be rearranged as follows [30]:

$$D_{ax}(r) = \frac{u(r) \cdot \Delta z}{2} \cdot \frac{\sigma_{t,i+1}^2(r) - \sigma_{t,i}^2(r)}{\Delta t_R^2(r)} \tag{10}$$

Index i denotes the number of the monitoring position. All variables of Eq. (10) were known from the CT experiments. So, for every single annulus in one segment of the column the HETP could be determined by Eq. (9), and consecutively its average value over the column cross section area could be calculated.

The dispersion resulting from the extra column effects did not need to be known, since it is the same at every monitoring position and it cancels out at the left side of Eq. (10). Namely, $(\sigma_{t,i+1}^2(r) + \sigma_{system}^2(r)) + (\sigma_{t,i}^2(r) + \sigma_{system}^2(r))$.

The tracer used in the CT experiments (KI) was a pore penetrating tracer, i.e. diffused in the pores of the particle. In the case of a pore penetrating tracer the parameter D_{ax} in Eq. (10) should be regarded as an apparent dispersion coefficient, D_{app}. The apparent dispersion coefficient is a lumped parameter, which accounts for the axial dispersion and the mass transfer kinetics. The objective of this work was to study the axial dispersion resulting strictly from the flow dynamics (packing structure). Therefore, the mobile phase flow rate in the CT experiments was selected near to the mobile phase flow rate corresponding to the minimum of the van-Deemter curve (minimal HETP). A preliminary analysis has shown that the contribution of the mass transfer kinetics to the apparent dispersion coefficient in the used range of mobile phase flow rate (3–6 ml/min) was negligible. Thus, even though the tracer used in the CT experiments was a pore-penetrating tracer, it could be assumed that the dispersion coefficient calculated by Eq. (10) is the axial dispersion coefficient.

3.1.2. Experimental results

The radial distribution of the parameters porosity and axial dispersion coefficient were already studied in the previous papers of the authors [4,5]. In these works the column was scanned at only four positions (5%, 35%, 65% and 95% of the column length), resulting in three segments along the column axis. Due to the limited number of segments, a general and reliable statement of the distribution of the studied parameters in axial direction was not possible. Therefore so far, the porosity and axial dispersion coefficient in axial direction were assumed to be constant. In this work, the distribution of the porosity and the axial dispersion coefficient in axial direction was closely examined, as the column was separated into nine segments.

In each segment between two monitoring positions, the porosity of the 40 annuli was calculated using Eqs. (4)–(8). In Fig. 4, the average value of the external porosity over the column cross sectional area in different segments along the column is presented.

As can be seen in Fig. 4, in the column packed with irregularly shaped particles as well as in the column with spherically shaped particles the value of the average external porosity varies slightly along the column axis, without a clear trend. In conclusion, the porosity in axial direction in both columns could be considered constant, i.e. around 0.29.

The procedure described in Section 3.1.1 was used to calculate the axial dispersion coefficient along the column. The obtained data are an averaged value over the column cross sectional area. In Fig. 5 the results of the evaluation for the two different stationary phases are presented.

The axial dispersion in the column of spherically shaped particles was slightly smaller than in the column packed with irregularly shaped particles. Both columns showed similar distribution of axial dispersion along the column axis. In both columns there was a slight increase of the axial dispersion coefficient along the column. This effect was more pronounced in the column packed with irregular shaped particles. Also, Guiochon and co-workers [24] have shown that the axial dispersion is higher at the end of the packed bed than in the other segments along the column. Further on, they observed a poor performance in the top part of the column. In our experiments the poor performance in the top section of the column was not observed.

In both columns, the axial dispersion coefficients determined at a flow rate of 6 ml/min were slightly higher than those calculated from CT experiments performed at a flow rate of 3 ml/min. In former experiments the influence of flow velocity on the HETP was studied. The HETP of the two columns was lowest (minimal) at a flow rate of 3 ml/min. By increasing the flow rate the influence of mass transfer kinetics on the band broadening, i.e. HETP increases. This is the reason for the slightly higher values of the axial dispersion coefficient obtained at a volumetric flow rate of 6 ml/min. Hence, the tracer used was a pore-penetrating tracer the calculated axial dispersion coefficients are actually the apparent dispersion

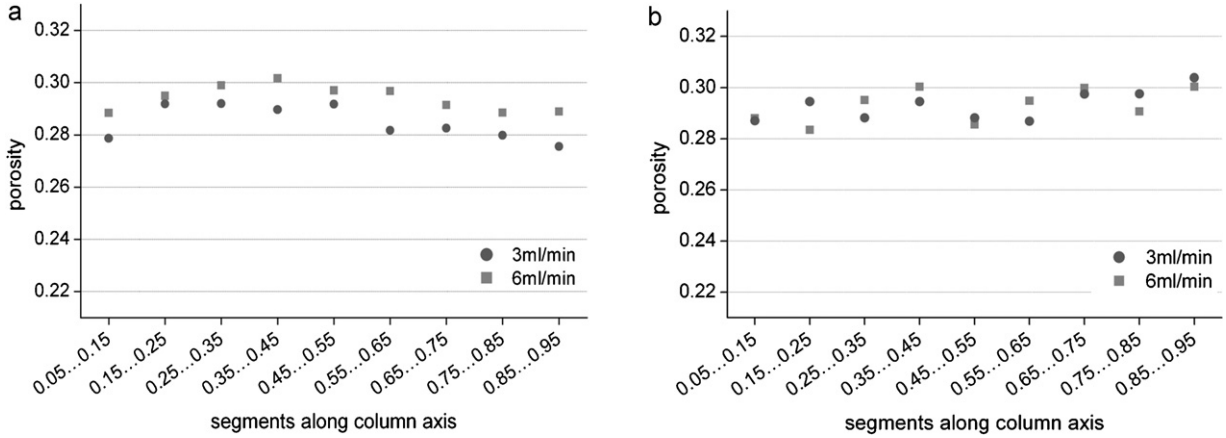

Fig. 4. Axial distribution of the porosity in columns packed with (a) irregularly shaped particles and (b) spherically shaped particles at mobile phase flow rates of 3 ml/min and 6 ml/min.

coefficients, in which all non-idealities like axial dispersion and mass transfer kinetics are summed up. The small difference between the axial dispersion coefficient at 3 ml/min and 6 ml/min suggested that the contribution of the mass transfer kinetics on the band broadening is insignificant. This conclusion was also supported by the fact that the tracer (KI) is a relatively small molecule with a high molecular diffusion coefficient (1.52×10^{-9} m^2 s^{-1}).

In summary, according to the results of the distribution of porosity and axial dispersion coefficient in axial direction, the column bed was of same homogeneity in both columns, whereas in radial direction the deviation of these parameter from the center of the column to the column wall was higher in case of irregular particles [5]. Therefore, the determination of the relevant parameters only in axial direction was not sufficient for the evaluation of the homogeneity of the column bed. The distribution in radial direction was more pronounced and gave clearer and more conclusive information about the packing quality of the column bed.

3.2. Simulation of chromatographic separation with Star-CCM+

CFD simulations are a reliable tool for conducting parameter studies and prediction of trends of process performances in a relatively short period of time. An important step in CFD simulations is the setup of the model including a correct implementation and adaptation to the special requirements of a particulate problem, in this work chromatographic separation processes. Once the model is setup, the only limiting factor for the calculation of the mathematical problem is the computational power. In this paper, only the equations of the model are presented. More information concerning CFD coding can be found in [32].

3.2.1. Setup of the model and model validation

The objective was to set up a CFD model of a chromatographic column which should help the user to select the right stationary phase for a particular separation task in advance. The data used in the simulation model to "generate" the porous structure of a chromatographic column was obtained from CT-experiments. The distribution of velocity and porosity, respectively, and axial dispersion were calculated by evaluating the CT images as explained in Section 3.1.1 using Eqs. (1)–(10). By implementing into the model the locally distributed data the radial and axial distribution of porosity and the axial dispersion coefficient was considered in the simulation of the flow pattern in the chromatographic column. Consecutively, the model could be used to perform simulations of a separation in columns packed with spherically and irregularly shaped particles and to select the right stationary phase for a particular separation task in advance.

Due to the rotational symmetry of a chromatographic column, a two-dimensional CFD-model was used. In the model, the following assumptions were considered: external porosity and axial

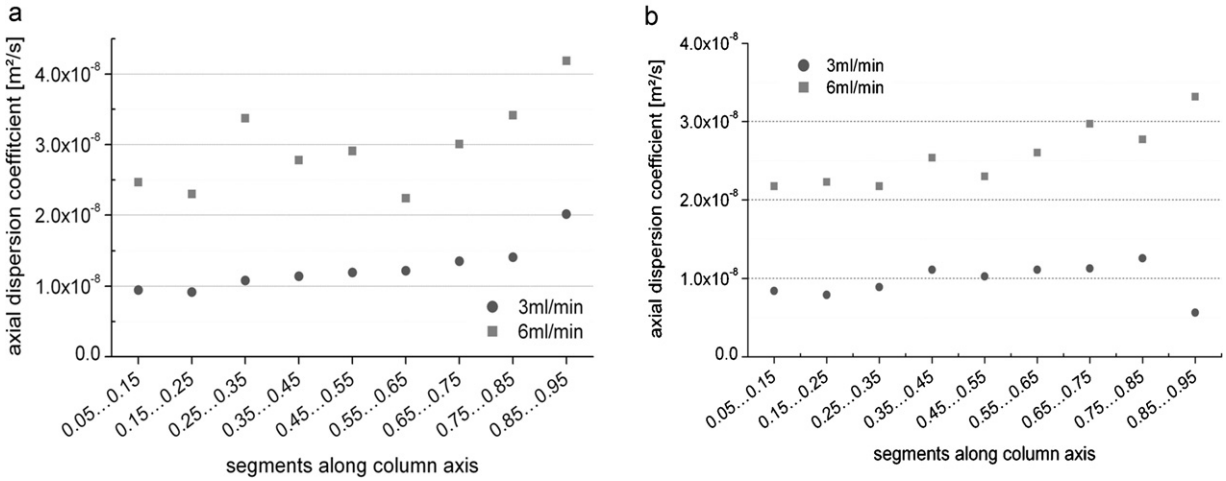

Fig. 5. Axial distribution of the axial dispersion coefficient in columns packed with (a) irregularly shaped particles and (b) spherically shaped particles at mobile phase flow rates of 3 ml/min and 6 ml/min.

dispersion coefficient are distributed in radial and axial direction whereas the liquid flow is only in axial direction. The interstitial velocity in axial direction is a function of the local porosity of the column. The transport equation, which is solved by the program Star-CCM+, was adjusted to account for the adsorptive interactions:

$$\frac{\partial c}{\partial t} + u \cdot \frac{\partial c}{\partial z} = D_{ax} \cdot \frac{\partial^2 c}{\partial z^2} - \frac{1-\varepsilon}{\varepsilon} \cdot \frac{\partial q}{\partial t} \quad (11)$$

In order to simulate a separation process close to reality the mass transfer between the mobile and the stationary phase had to be described and included into the CFD model. One relatively simple approach was to replace the axial dispersion coefficient in Eq. (11) with apparent dispersion coefficient, D_{app}, which sum up the axial dispersion and all mass transfer non-idealities [27]. For each annulus in every segment of the column, the apparent dispersion coefficient was calculated following Eq. (12)

$$D_{app}(r) = D_{ax}(r) + \left(\frac{\tilde{k}'}{1+\tilde{k}'}\right)^2 \cdot \frac{\varepsilon(r)}{(1-\varepsilon(r))} \cdot \frac{r_p \cdot u(r)^2}{3 \cdot k_{eff}} \quad (12)$$

In this equation the parameters D_{ax} and ε were obtained from CT experiments, all other parameters were calculated according to common correlations as explained in [27]. It should be mentioned that the distinction of the particle's geometry was only given by the distribution of the parameters obtained by CT experiments, i.e. the external porosity, axial distribution coefficient and interstitial velocity. For calculation of the apparent dispersion coefficient, the mean diameter of the particles was used. In the simulation of a separation task performed in a column of irregular particles the geometry of the particles was considered as spherical.

The adsorption equilibrium was described by the multi-component Langmuir isotherm.

$$q_i = q_{sat} \cdot \frac{b_i c_i}{1 + \sum_{j=1}^{n} b_j c_j} \quad (13)$$

The simulations were carried out on one node of a high performance computer. One node consists of two Xeon 5160 "woodcrest" chips (4 cores) of 3.0 GHz with 4 MB shared level 2 cache per dual core, 8 GB RAM and a 160 GB local scratch disk. The CPU time for one simulation took 8–12 h depending on the used set of model parameters.

In our previous work, the radial distribution of porosity, interstitial velocity and axial dispersion coefficient, determined experimentally from CT experiments, was implemented into the CFD model, but the distribution of these parameters along the column axis was kept constant [5]. Here the axial as well as the radial distribution detected in the CT measurements have been taken into account. Therefore, a program in MATLAB was created to sort the experimental values of the porosity and axial dispersion obtained for every single annulus and segment. The data was written in tables consisting of columns with the spatial distribution in *r*- and *z*-direction with the associated values for porosity and axial dispersion coefficient. These data were used as hydrodynamic input parameters in the CFD model. In each annulus and segment the interstitial velocity was calculated from the flow rate and local value of the porosity.

First, two simulations of a pulse injection of a pore penetrating non-adsorbing tracer were carried out and the results were compared to each other. In the first simulation run, only the radial distribution of porosity and axial dispersion coefficient was taken into account. In the second run, the distribution of these parameters in both directions, axial and radial, was considered. The discretization parameters used in the CFD model and the chromatographic model parameters used for the simulation are summarized in Table 2.

Table 2
Parameters used for the simulation of elution profiles of a pulse injection with a pore penetrating non-adsorbing tracer.

Parameter	
CFD model parameter	
Total number of cells [–]	62,400
Cell width [m]	2.5×10^{-4}
Time step [s]	0.3
Separation process parameter	
Superficial velocity [m s^{-1}]	5×10^{-4}
Inlet concentration c_i [kg/m^3]	31.45
Injection volume [m^3]	0.7×10^{-6}
Bed length [m]	0.302
Column averaged D_{ax} [m^2 s^{-1}]	2.63×10^{-8}
Average external porosity ε	0.29

In Fig. 6, the concentration elution profile of the tracer obtained when only radial distribution of the external porosity and axial dispersion was considered is compared to the elution profile obtained when both, radial and axial distribution of these parameters were considered. As can be seen from the figure, both elution peaks are almost identical. The slight change of the external porosity and axial dispersion coefficient in axial direction determined by CT measurements did not considerably affect the elution profile of the tracer. The assumption of the author's in the previous works [4,5] that porosity and axial dispersion coefficient along the column axis can be considered constant was also proven by the simulation.

Referring to this, one can conclude that in the semi-preparative columns used in these experiments, the axial distribution of the parameters porosity and axial dispersion coefficient is negligible compared to their radial distribution. This is not a general statement, as in columns of larger diameter or column length the distribution of these parameters may be different.

3.2.2. Prediction of separation performances and selection of stationary phase

To demonstrate the applicability and benefit of the developed CFD model (Eqs. (11)–(14)), the model was used to simulate a batch elution separation of a mixture of two model components in a column packed with spherically and irregularly shaped particles of same size. The aim was to select the most suitable stationary phase in terms of separation performance (yield), for a binary

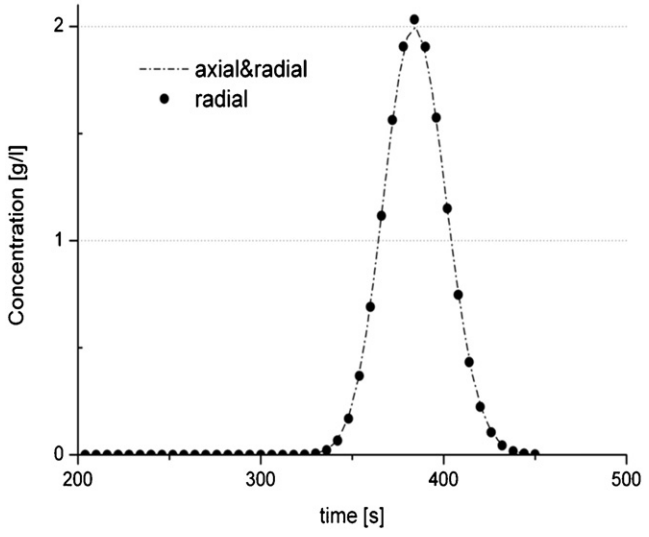

Fig. 6. Chromatogram of the pulse injection of a pore penetrating non-adsorbing tracer in a column of spherically shaped particles with radial distribution of porosity and axial dispersion coefficient (dotted line) and radial distribution combined with axial distribution of porosity and axial dispersion coefficient (straight line).

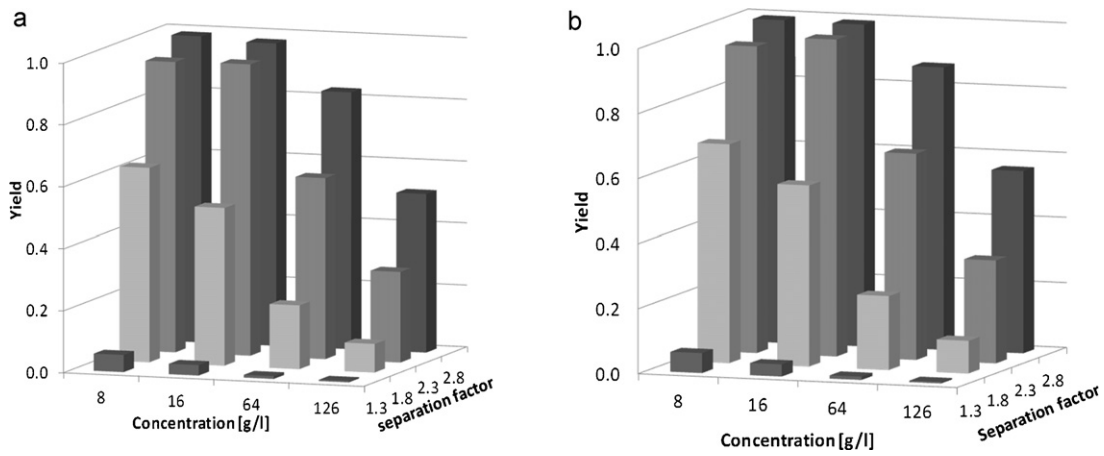

Fig. 7. Three dimensional plot of total yield for different feed mixture concentrations and separation factors for (a) irregularly shaped particles and (b) spherically shaped particles, with a particle size of 50 μm.

mixture with given solute concentration and/or separation factor. The porous structure of the columns was generated by using the radial distribution of porosity and the axial dispersion coefficient obtained by CT experiments. The product purity requirements were set to nearly 100% for both compounds. The concentration of the mixture, in the following text referred to as feed concentration, was varied in a range between 8 g/l and 126 g/l for each component. The separation factor, which was defined according to Eq. (14), was varied in a range between 1.3 and 2.8. The different separation factors were achieved by changing the Langmuir coefficient b.

$$\alpha = \frac{q_{\mathrm{sat},j} \cdot b_j}{q_{\mathrm{sat},i} \cdot b_i} \tag{14}$$

Table 3 summarizes the model parameters used in the CFD simulations. The CFD model discretization parameters are as listed in Table 2.

The results of the simulations are presented in three dimensional plots, where the total yield obtained for different combinations of the feed mixture concentration and separation factor can be read. In Fig. 7, the results are shown for irregularly and spherically shaped particles with a particle size of 50 μm.

On the first sight the distribution of the total yield over the two variables, feed concentration and separation factor, was the same in the two columns packed with stationary phases of different particle geometry. As expected, with the increase of the feed concentrations the total yield decreased and with the increase of the separation factor the total yield also increased. Table 4 gives an overview of the benefit of using spherically shaped particles with particle size of 50 μm compared to irregularly shaped particles of same size.

In every single case the total yield obtained in the column packed with spherically shaped particles was higher than in the column packed with irregularly shaped particles. The difference in yield decreased with increasing separation factors, except for a feed concentration of 126 g/l. Here, the total yields were constant at

Table 3
CFD model parameters used for simulation of a binary mixture separation in a columns packed with spherical and irregular shaped particles.

Parameter	
Superficial velocity [m s^{-1}]	5×10^{-4}
Particle size [m]	20×10^{-6}
	50×10^{-6}
Sample concentration c_i [kg/m^3]	8
	16
	64
	126
Injection volume [m^3]	0.7×10^{-6}
Bed length [m]	0.28
q_{sat} [g/l]	12
b1	0.1
b2	$0.077 \rightarrow \alpha = 1.3$
	$0.056 \rightarrow \alpha = 1.8$
	$0.043 \rightarrow \alpha = 2.3$
	$0.036 \rightarrow \alpha = 2.8$

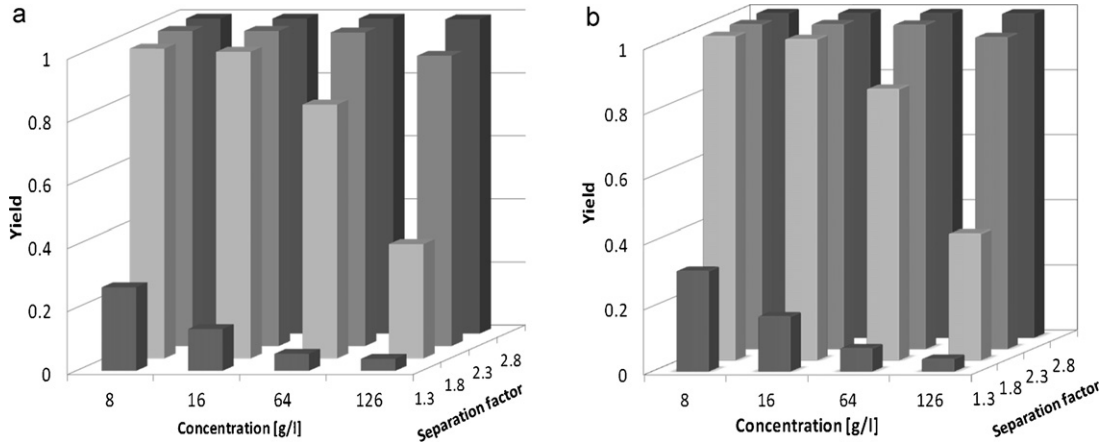

Fig. 8. Three dimensional plot of total yield for different feed mixture concentrations and separation factors for (a) irregularly shaped particle sand (b) spherically shaped particles, with a particle size of 20 μm.

Table 4
Percental increase of total yield obtained when spherically shaped particles are used instead of irregularly shaped particles.

Inlet concentration [g/l]	Separation factor			
	1.3	1.8	2.3	2.8
8	10.6	7.2	0.6	0.4
16	11.1	9.4	3.6	1.4
64	12.5	10.5	8.5	4.8
126	8.9	8.8	8.2	9.5

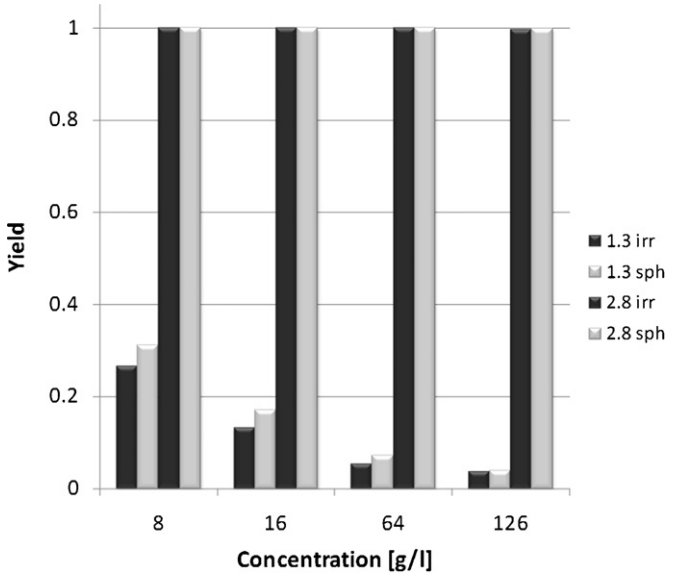

Fig. 9. Total yield in columns with particle sizes of 20 μm; base line separation occurs at separation factors above 2.

different separation factors. The reason was that this feed concentration is far in the saturated region of the multicomponent Langmuir isotherm. In this region the separation was controlled by the thermodynamics rather than by mass transfer and column hydrodynamics.

For particles with a particle size of 20 μm the distribution of total yield is shown in Fig. 8.

Again, the course of total yield looked similar in both columns. The yield obtained in a column packed with spherically shaped particles was again higher than the one obtained in a column packed with irregular ones. In columns packed with smaller particles the feed concentration had only an influence on the separation at low separation factors (around 1.3). In chromatographic systems having separation factors above 2 independent of the feed concentration, a base line separation was reached (see Fig. 9). In these cases the choice of a stationary phase of irregularly shaped particles is justified.

The plots in Figs. 7 and 8 shall help to choose the appropriate stationary phase for a given separation task. Namely, for a given feed concentration and separation factor, the total yield for the separation in a column of spherically shaped particles and a column of irregularly shaped particles can be read from the plots and the best suited stationary phase can be selected.

4. Conclusions

The X-ray computed tomography was used to study the homogeneity of the packed bed of chromatographic columns made of spherically and irregularly shaped stationary phase particles of same size.

The axial and radial distribution of the bed porosity and axial dispersion coefficient was estimated from the breakthrough curves of a tracer recorded at ten monitoring positions along the column. Focus was given to the axial distribution of these parameters, since their radial distribution had been deeply studied in our previous works. The average value of the porosity and axial dispersion coefficient across the column cross sectional area showed no significant change along the column axis. The CFD simulation of the tracer elution profile at the column outlet had also shown that, in comparison to the radial distribution, the observed change of the porosity and axial dispersion coefficient in axial direction was insignificant, and did not affect the shape of the elution peak. In summary, for a rough estimation of the distribution of porosity and axial dispersion constant in radial and axial direction only four CT monitoring positions could be used.

To reduce experimental effort for selecting the best suited packing material for a particular separation problem, a CFD model with the locally distributed porosity and axial dispersion coefficient obtained from CT measurements could be used. To demonstrate this, the total yield of a separation of a binary model mixture, with different concentration and separation factor, was determined. The resulting plots representing the total yield in dependence of the mixture (feed) concentrations and separation factors should help to select the right stationary phase for a particulate separation task in advance.

Nomenclature

α	[–] separation factor
A_C	[m^2] column cross section
b	[–] Langmuir coefficient
c	[$g\,L^{-1}$] concentration
CT	[–] CT-number
d_P	[m] particle diameter
D_C	[m] column diameter
D	[$m^2\,s^{-1}$] dispersion coefficient
D_{ax}	[$m^2\,s^{-1}$] axial dispersion coefficient
D_{app}	[$m^2\,s^{-1}$] apparent dispersion coefficient
ε	[–] external porosity
ε_p	[–] particle porosity
ε_t	[–] average total porosity
HETP	[m] height equivalent of a theoretical plate
$\tilde{k}'$	[–] modified retention factor
k_{eff}	[–] effective mass transfer coefficient
L	[m] column length
μ	[$kg\,m^{-1}\,s^{-1}$] dynamic viscosity
p	[bar] pressure
q	[$g\,L^{-1}$] solid load
q_{sat}	[$g\,L^{-1}$] saturation capacity of the stationary phase
r	[m] radial position
r_P	[m] particle radius
σ^2	[s^2] variance
S	[–] saturation
t	[s] time
t_R	[s] retention time
u	[$m\,s^{-1}$] interstitial velocity
u_0	[$m\,s^{-1}$] superficial velocity
v_{KI}	[$m\,s^{-1}$] tracer velocity
$\bar{v}_{KI}$	[$m\,s^{-1}$] averaged tracer velocity
$\dot{V}$	[$m^3\,s^{-1}$] volumetric flow
z	[m] axial position

Indices

SP	stationary phase
MP	mobile phase
i	measuring position
i	component

0	start time
1	component 1
2	component 2

References

[1] T. Farkas, M. Sepaniak, G. Guiochon, J. Chromatogr. A 740 (1996) 169.
[2] T. Farkas, J.Q. Chambers, G. Guiochon, J. Chromatogr. A 679 (1994) 231.
[3] D.U. Astrath, F. Lottes, D.T. Vu, W. Arlt, E.H. Stenby, Adsorption 13 (2007) 9.
[4] F. Lottes, et al., J. Chromatogr. A 1216 (2009) 5687.
[5] I. Schmidt, F. Lottes, M. Minceva, W. Arlt, E.H. Stenby, Chem. Ing. Tech. 83 (1–2) (2011) 130.
[6] J.E. Baur, E.W. Kristensen, R.M. Wightman, Anal. Chem. 60 (1988) 2334.
[7] U. Tallarek, J. Chromatogr. A 696 (1995) 1.
[8] T. Farkas, M. Sepaniak, G. Guiochon, Anal. Chem. 69 (1997) 647A.
[9] G. Guiochon, J. Chromatogr. A 762 (1997) 83.
[10] K. Kaczmarski, F. Gritti, J. Kostkaa, G. Guiochon, J. Chromatogr. A 1216 (2009) 6575.
[11] F. Gritti, G. Guiochon, J. Chromatogr. A 1217 (2010) 5137.
[12] G. Guiochon, E.C. Drumm, D. Cherrak, J. Chromatogr. A 835 (1999) 41.
[13] B.G. Yew, E.C. Drumm, G. Guiochon, AIChE J. 49 (2003) 626.
[14] B.G. Yew, J. Ureta, R.A. Shalliker, E.C. Drumm, G. Guiochon, AIChE J. 49 (2003) 642.
[15] R.F. Benenati, C.B. Brosilow, AIChE J. 8 (1962) 359.
[16] B. Porsch, J. Chromatogr. A 658 (1994) 179.
[17] J. Billen, P. Gzil, N. Vervoort, G.V. Baron, G. Desmet, J. Chromatogr. A 1073 (2005) 53.
[18] S. Harding, J. Chromatogr. 905 (2001) 19.
[19] U. Tallarek, K. Albert, E. Bayer, G. Guiochon, AIChE J. 42 (1996) 3041.
[20] U. Tallarek, E. Bayer, D. van Dusschoten, T. Scheenen, H. van As, G. Guiochon, U.D. Neue, AIChE J. 44 (1998) 1962.
[21] U. Tallarek, D. van Dusschoten, H. van As, E. Bayer, G. Guiochon, J. Phys. Chem. B 102 (1998) 3486.
[22] T. Laiblin, W. Arlt, R. Kaiser, R. Kirsch, Chem. Ing. Tech. 79 (2007) 1213.
[23] J. Chaouki, F. Larachi, M. Dudukovic, Ind. Eng. Chem. Res. 36 (1997) 4476.
[24] V. Wong, R.A. Shalliker, G. Guiochon, Anal. Chem. 76 (2004) 2601.
[25] R.A. Shalliker, B.S. Broyles, G. Guiochon, J. Chromatogr. A 994 (2003) 1.
[26] A. Mottlau, Anal. Chem. 34 (1962) 714.
[27] H. Schmidt-Traub, Preparative Chromatography of Fine Chemicals and Pharmaceutical Agents, Wiley-VCH, Weinheim, 2005.
[28] E. Baumeister, U. Klose, K. Albert, E. Bayer, G. Guiochon, J. Chromatogr. A 694 (1995) 321.
[29] D.U. Astrath, Dissertation, Friedrich-Alexander Universität Erlangen-Nürnberg, 2007.
[30] O. Levenspiel, Chemical Reaction Engineering, 2nd ed., Wiley, New York, 1972.
[32] H.K. Versteeg, W. Malalasekera, An Introduction to Computational Fluid Dynamics: The Finite Volume Method, Pearson Education Ltd., England, 2007.
[33] S. Khirevich, A. Höltzel, A. Seidel-Morgenstern, U. Tallarek, Anal. Chem. 81 (2009) 7057.
[34] U.M. Scheven, AIChE J. 56 (2010) 289.
[35] H. Guo, D.D. Frey, J. Chromatogr. A 1217 (2010) 6214.
[36] T. Atmakidis, E.Y. Kenig, Chem. Eng. J. 155 (2009) 404.
[37] F. Augier, F. Idoux, J.Y. Delenne, Chem. Eng. Sci. 68 (2010) 1055.
[38] P. Gzil, N. Vervoort, G.V. Baron, G. Desmet, Anal. Chem. 75 (2003) 6244.
[39] P. Gzil, J. De Smet, N. Vervoort, H. Verelst, G.V. Baron, G. Desmet, J. Chromatogr. A 1030 (2004) 53.
[40] J. De Smet, P. Gzil, N. Vervoort, H. Verelst, G.V. Baron, G. Desmet, J. Chromatogr. A 1073 (2005) 43.

Further reading

[31] W.A. Kalender, Computed Tomography: Fundamentals, System Technology, Image Quality, Applications, Publicis Corporate Publishing, Erlangen, 2005.